Fabrication of flower-shaped Bi_2O_3 superstructure by a facile template-free process

Li Zhang [a], Yoshio Hashimoto [a], Toshinori Taishi [a], Isao Nakamura [b], Qing-Qing Ni [b,*]

[a] Faculty of Engineering, Shinshu University, Japan

[b] Dept. of Functional Machinery & Mechanics, Shinshu University, Japan

Abstract

A novel flower-shaped Bi_2O_3 superstructure has been successfully synthesized by calcination of the precursor, which was prepared via a citric acid assisted hydrothermal process. The precursor and Bi_2O_3 were characterized with respect to morphology, crystal structure and elemental chemical state by field-emission scanning electron microscopy (FESEM), transmission electron microscopy (TEM), X-ray diffraction (XRD) and X-ray photoelectron spectroscopy (XPS). It was shown that both the precursor and Bi_2O_3 flower-shaped superstructure were constructed of numerous nanosheets while the nanosheets consisted of a great deal of nanoparticles. Furthermore, key factors for the formation of the superstructures have been proposed; a mechanism for the growth of the superstructure has been presented based on the FESEM investigation of different growth stages.

Keyword: Bi_2O_3; superstructure; Hydrothermal

[*] Corresponding author at: Dept. of Functional Machinery & Mechanics, Shinshu University, 3-15-1 Tokida, Ueda 386-8567, Japan. Tel/Fax: +81 268 21 5438
E-mail address: niqq@shinshu-u.ac.jp (Qing-Qing Ni)

Introduction

Over the past few years, considerable interest has been focused on the synthesis of nanostructures with controllable morphologies because of the strong relationship between the structures and their attractive physical or chemical properties [1-7]. Due to the unique structural and surface properties, inorganic three-dimensional (3D) spherical structures with nanometer to micrometer size, which assembled from low dimensional nanostructure, are proposed to have potential applications in catalysis, chemical sensors, photocatalysis, controlled delivery and release of drugs, and so on [8-12]. A variety of methods have been employed to prepare the spherical structures of inorganic materials, and the template method is the classical synthetic approach [13-16]. However, the template-assisted process falls short of the practical significance due to the introduction of heterogeneous impurities as well as the increased production cost. Under certain conditions, nanoparticles can undergo self-assembly to form spherical superstructure, and many self-assemble processes have been attempted to prepare inorganic materials with 3D spherical structures [17-20]. Herein, we report a novel and facile approach to synthesize Bi_2O_3 spherical flower-like structure using a citric acid (CA) assisted hydrothermal process in combination with subsequent calcination.

Bi_2O_3, an important metal oxide semiconductor with a direct band gap of 2.8 eV, has been receiving considerable attention because of its various applications, such as photocatalyst, solid oxide fuel cell, gas sensor and ion conductive solid electrolyte [21-27]. Recent years, several successful strategies including precipitation method [28-30], microwave-assisted synthesis [31], electrodepositon route [32,33], and chemical vapor deposition (CVD) [34,35], have been reported to prepare Bi_2O_3 with various morphologies, such as Quantum dots [28], nanoparticles [30], nanobelts [27], nanorods [34,35], nanotubes [36], nanofibers [37] and film [32]. Here, we report a facile and template-free process to prepare 3D spherical superstructure. Due to simplicity, low cost, and suitability for eco-friendly large-scale production, the process reported here should be a promising synthesis route for Bi_2O_3 superstructure.

Experimental

All reagents were of analytical grade without further purification. In a typical experiment, 0.97 g bismuth nitrate ($Bi(NO_3)_3 \cdot 5H_2O$, 2 mmol) and 0.13 g citric acid

(CA, $C_6O_7H_8$, 0.67 mmol) were dissolved in 40 mL of nitric acid (1 M) to form a clear solution. The pH of the solution was adjusted to 6 with adding KOH (8 M) solution under stirring. The pH was measured using a TPX-999 pH meter (Toko Chemical Laboratories Co., Ltd.). After 10 min of stirring, the aforementioned solution was transferred into a Teflon-lined stainless steel reaction autoclave (capacity 50 mL) and sealed. The autoclave was heated at 200 ˚C for 12 h and then cooled naturally to room temperature. The precursor was centrifuged, filtered out, and rinsed with deionized water and alcohol several times and than dried at 60 ˚C overnight. Finally, the Bi_2O_3 sample was obtained by calcination of the precursor in a tube oven at 400 ˚C for 3 h in air atmosphere.

Phase identification of the samples was carried out by X-ray powder diffraction (XRD) using a Rigaku Geigerflex 2028 diffractometer with Cu Kα radiation (λ = 1.5418 Å). Morphology observation was performed on field emission scanning electron microscopy (FESEM, Hitachi S-5000, 20 kV) and transmission electron microscopy (TEM, JEOL JEM-2010, 200 kV). X-ray photoelectron spectroscopy (XPS) analysis was measured with a Kratos Axis Ultra DLD X-ray photoelectron spectrometer using a standard Mg Kα (1256.6 eV) X-ray source (10 mA, 15 kV) and low-energy electron flooding for charge compensation, and all binding energies were referred to Au $4f_{7/2}$ at 83.8 eV. Thermogravimetrical analysis (TGA) was performed on a Rigaku Thermo Plus TG8120 apparatus (Rigaku Denki, Japan) under air atmosphere at 10 °C/min in a temperature rang of 30–550 °C.

Results and discussion

FESEM and TEM were used to characterize the morphologies of the precursor. Figure 1 gives the morphologies of as-prepared precursor (hydrothermally treated at 200 °C for 12 h, $Bi(NO_3)_3$:CA molar ratio of 3:1, pH = 6). As shown in Figure 1a, all the precursors have a spherical morphology, with an average diameter of 6 μm. The magnified FESEM image (Figure 1b) indicates that the precursor samples possess a hierarchical structure of a flower-shaped appearance. Interestingly, the superstructures are in fact assembled from nanosheets (inset of Figure 1b). Further information about the precursor was obtained from TEM images. They confirmed that the precursor sphere have diameters around 6 μm (Figure 1c), consistent with the value shown in the FESEM images. Simultaneously, the nanosheets (Figure 1d, the substructure of

the sphere architecture) are assembled from thousands of nanoparticles. Moreover, the HRTEM investigation (Figure 1e) demonstrates that the nanoparticles show its crystalline nature, and have a diameter around 10 nm.

Citric acid (CA) is a versatile, widely used, and safe capping agent. In our case, the hydrothermal temperature, CA concentration, reaction time and pH play critical roles in hydrothermal formation of flower-shaped precursor sphere. To verify the effect of temperature, we conducted the hydrothermal process at 160, 180, 200 and 220 °C, respectively. As shown in Figure 2a, the flower-like precursors were not formed at 180 °C. When the temperature reached 200 °C, the flower-like precursors turned to be the main component. However, the hydrothermal temperature made no difference in the shape of the precursor over 200 °C by the comparison of Figure 2b with Figure 1b. Generally, the temperature dependence of the material structure is quite complicated, and a suitable hydrothermal temperature is required for the preparation of product with specific structure, which is 200 °C in our case. The increase of hydrothermal temperature causes a significant increase in ambient pressure, and in our experiments, such an increase in environmental pressure may be favorable for the formation of the flower-like precursors. Moreover, the shape changed with the concentration of CA. Figure 3a shows that the precursors synthesized with a high concentration of CA (the molar ratio of $Bi(NO_3)_3$:CA was 1:1) had obvious broaden diameter ranging from few microns to decades of microns. While there was low CA concentration, the precursors tended to have two structures, flower-like sphere and irregular-shaped crystal. Formation of irregular-shaped crystal can be due to shortage of CA to cap with Bi^{3+} to yield bismuth citrate complexes. When no CA was added, the precursor only showed irregular-shaped crystal with a diameter of decades of microns, as shown in Figure 3b. Therefore, CA is extremely critical for the formation of flower-like sphere. Meanwhile, the shape of precursor changed with the pH of the final solution. When pH ≥ 4, flower-like sphere could be obtained. Upon decreasing the pH in the range of 0.6–1.2, irregular-shaped crystal with a diameter of decades of microns instead of flower-like sphere were obtained (the FESEM image is similar with Figure 3b). At the optimized condition ($Bi(NO_3)_3$:CA molar ratio of 3:1, pH = 6, 200 °C), we found that it was still not enough to form flower-shaped sphere with uniform size and structural integrity within 6 h (see Figure 3c). Moreover, the formed flower-shaped sphere of Figure 3c was still immature with incomplete crystallization (inset of Figure 3c).

However, it seems to have little effect on the mean diameters of the flower-shaped spheres when prolonged the reaction time to 24 h (Figure 3d).

To investigate the appropriate calcination temperature for the transformation of precursor to Bi_2O_3, we conducted the TG analysis in air atmosphere. The TGA and the corresponding differential thermogravimetric (DTG) curves are shown in Figure 4. The weight loss was located in the temperature range of 200–380 °C, which can be attributed to the removal of amorphous residue and the mass loss of phase transformation from precursor to Bi_2O_3. We calculated the temperature at maximal weight loss rate (T_{mwlr}) form its DTG curve and found that T_{mwlr} was around 350 °C. Therefore, the temperature of 400 °C was chosen for calcination process to ensure the complete phase transformation.

The crystal structures of the samples were characterized by XRD, and their patterns are shown in Figure 5. Figure 5a shows the XRD pattern of precursor obtained in the hydrothermal step. All the peaks of precursor were in good agreement with the value of tetragonal bismutite ($Bi_2(CO_3)O_2$, JCPDS no. 25-1464, see Figure 5b). Subsequent to calcination of the precursor at 400 ˚C for 2 h, all XRD peaks could be indexed to monoclinic bismite (Bi_2O_3) with lattice constants a = 5.85 Å, b = 8.17 Å, c = 7.51 Å (see Figure 5c), which matched well with values from the standard card (JCPDS no. 71-2274, see Figure 5d). Generally, Bi_2O_3 is a complex system with four main polymorphs: α (monoclinic), β (tetragonal), γ (body-centered cubic) and δ (face-centered cubic), and the α and β phases are the stable phases at both room and high temperature [29]. As shown in Figure 5, XRD patterns before and after calcination have substantial difference both in the peak locations and the peak amounts, indicating that the precursor has been transformed to α–Bi_2O_3 after calcination process. We calculated the particle sizes of the precursor and Bi_2O_3 using the Scherer formula, $D = 0.89\lambda/(\beta\cos\theta)$, where λ is the X-ray wavelength (1.5418 Å), θ is the Bragg diffraction angle, and β is the experimental full width at half maximum (fwhm) of the respective diffraction peaks. The crystallite sizes of the precursor and Bi_2O_3 were estimated to 10 nm and 21 nm, respectively.

XRD results confirm that the Bi_2O_3 was obtained by calcination of the precursor at 400 °C for 3h. The effect of calcination on the morphology was also investigated by

FESEM and TEM. As expected, the overall appearance of both flower-shaped sphere and sphere diameter was successfully kept (Figure 6a and 6b). TEM image (Figure 6c) revealed that the Bi_2O_3 had a diameter of 6 μm and flower-shaped appearance, which was in good agreement with the size and shape of precursor. A TEM image at higher magnification indicated that the obtained Bi_2O_3 was composed by nanocrystals with the size of 20–30 nm which agreed well with XRD result (Figure 6d), and HRTEM image (Figure 6e) further revealed the crystal structure of the nanocrystals. Notably, as shown in the HRTEM image, numerous nanopores existed among these nanocrystals, which was created by the released gas during the calcination process. The clear lattice fringe indicated the crystalline nature of the Bi_2O_3 nanoparticles. The interplanar spacings were 0.347 nm and 0.317 nm, which corresponded to the (002) and (012) planes of monoclinic Bi_2O_3, respectively.

To elucidate the elemental compositions and the chemical state of Bi in the precursor and Bi_2O_3, we carried out XPS analysis and present the typical XPS spectra in Figure 7. Wide scans (Figure 7a) of the precursor and Bi_2O_3 indentified the presence of bismuth (Bi 4f, Bi 4d, Bi 4p, Bi 5d), oxygen (O 1s) and carbon (C 1s). The concentration of carbon clearly decreased after calcination process because of the phase transformation from $Bi_2(CO_3)O_2$ (precursor) to Bi_2O_3 and the removal of the amorphous carbon generated during hydrothermal process. Figure 7b shows the high-resolution spectra of Bi 4f. For the spectra of precursor, double peaks with binding energies of 159.3 and 164.6 eV corresponded to Bi $4f_{7/2}$ and Bi $4f_{5/2}$ of $Bi_2(CO_3)O_2$, respectively. However, the binding energies of Bi 4f shifted toward the low-energy side after calcination, the values were 158.8 eV for Bi $4f_{7/2}$ and 164.1 eV for Bi $4f_{5/2}$, which agreed with the literature data for commercial bismuth oxide [23]. The shift of binding energies confirms the complete phase transformation from $Bi_2(CO_3)O_2$ to Bi_2O_3 after calcination process (400 °C, 3h).

Hydrothermal method has sparked much interest in recent years, due to its operational simplicity, and capability for large-scale production. The hydrothermal method reported here without the need for tedious process and rigorous conditions can be considered as a low-cost and convenient method to prepare flower-shaped Bi_2O_3 structure. In order to investigate the growth mechanism of the flower-like Bi_2O_3 sphere, the growth processes of precursor were carefully studied by analyzing the

samples at different growth stage. Figure 8 shows a series of FESEM images of the precursor by varying the reaction time at 2, 6 and 12 h (other reaction conditions: $Bi(NO_3)_3$:CA molar ratio of 3:1; pH=6; 200 °C). As shown in Figure 8a, the precursor was composed of loosely assembled colloid nanostructures, while the nanostructure were observed to consist of a great deal of nanoparticles (inset of Figure 8a). Figure 8b shows that many loose colloid nanostructures were assembled to form spherical precursors although the precursors did not have uniform size and structural integrity. In addition, the loose nanostructure could still be found everywhere (inset of Figure 8b). Subsequently, on increasing the hydrothermal treatment time to 12 h, almost all the colloid nanostructures were transformed to flower-shaped spherical structure with uniform size. On the basis of the above discussion it can be concluded that formation of flower-like spherical precursor is due to a cooperation effect of classical Ostwald ripening and self-assembly process [19]. Finally, the flower-shape spherical Bi_2O_3 with nanopore structure were obtained after the subsequent calcination process.

Conclusions

Bi_2O_3 with unique flower-like spherical structure has been successfully prepared by a facile and template-free method. The morphology, crystal structure and elemental chemical state of precursor and Bi_2O_3 were systematically characterized by FESEM, TEM, XRD and XPS. The flower-like spherical Bi_2O_3 were assembled from thousands of Bi_2O_3 nanoparticles with an approximate diameter of 20 nm. A growth mechanism for the precursor and Bi_2O_3 has been clearly presented. Moreover, we found that hydrothermal temperature, citric acid concentration and pH are the key factors for the formation of flower-shaped precursor.

References

[1] H. Goesmann, C. Feldmann, Angew. Chem. Int. Ed. 49 (2009) 1362.

[2] L.Y. Chen, Y. Shen, J. Bai, C. Wang, J. Solid State Chem. 182 (2009) 2298.

[3] X.J. Wu, F. Zhu, C. Mu, Y. Liang, L. Xu, Q. Xhen, R. Chen, D. Xu, Coord. Chem. Rev. 245 (2010) 1135.

[4] L. Chen, Z. Xu, H. Dai, S. Zhang, J. Alloys Compd. 497 (2010) 221.

[5] J. Lin, Y. Huang, Y. Bando, C. Tang, C. Li, D. Golberg, Acs Nano 4 (2010) 2452.

[6] Y. Liu, W. Wongwiriyapan, K.C. Park, H. Muramatsu, K. Takeuchi, Y.A. Kim, M. Endo, Carbon 47 (2009) 2543.

[7] H. Zhu, H. Hu, Z. Wang, D. Zuo, Nanoscale Res. Lett. 4 (2009) 1009.

[8] H. Liang, H. Yang, W. Wang, J. Li, H. Xu, J. Am. Chem. Soc. 131 (2009) 6068.

[9] L.Y Chen, H. Dai, Y. Shen, J. Bai, J. Alloys Compd. 491 (2010) L33.

[10] N.C. Strandwitz, G.D. Stucky, Chem. Mater. 21 (2009) 4577.

[11] M. Srinivasarao, D. Collings, A. Philips, S. Patel, Science 292 (2001) 79.

[12] H. Zhu, D. Zuo, J. Phys. Chem. C 113 (2009) 10402.

[13] X. Guo, Y. Deng, B. Tu, D. Zhao, Langmuir 26 (2010) 702.

[14] A. Ajayaghosh, R. Varghese, V.K. Praveen, S. Mahesh, Angew. Chem. Int. Ed. 45 (2006) 3261.

[15] Z. Yang, Z. Niu, Y. Lu, Z. Hu, C.C. Han, Angew. Chem. Int. Ed. 42 (2003) 1943.

[16] X. Sun, J. Liu, Y. Li, Chem. Eur. J. 12 (2006) 2039.

[17] D. Wu, H. Zhu, C. Zhang, L. Chen, Chem. Commun. 46 (2010) 7250.

[18] X.J. Dai, Y.S. Luo, W.D. Zhang, S.Y. Fu, Dalton Trans. 39 (2010) 3426.

[19] L. Zhang, W. Wang, Z. Chen, L. Zhou, H. Xu, W. Zhu, J. Mater. Chem 17 (2007) 2526.

[20] F. Zhang, D. Zhao, Nano Res. 2 (2009) 292.

[21] Y. Gong, W. Ji, L. Zhang, B. Xie, H. Wang, J. Power Sources 196 (2011) 928.

[22] P. Malik, D. Chakraborty, Tetrahedron Lett. 51 (2010) 3521.

[23] R. Li, W. Chen, H. Kobayashi, C. Ma, Green Chem. 12 (2010) 212.

[24] L. Zhou, W. Wang, H. Xu, S. Sun, M. Shang, Chem. Eur. J. 15 (2009) 1776.

[25] C. Hong, H.W. Kim, W.I. Lee, C. Lee, Thin solid Films 518 (2010) 6638.

[26] D. Yuan, J. Zeng, N. Kristian, Y. Wang, X. Wang, Electrochem. Commun. 11 (2009) 313.

[27] F.L. Zheng, G.R. Li, Y.N. Ou, Z.L. Wang, C.Y. Su, Y.X. Tong, Chem. Commun. 46 (2010) 5021.

[28] H. Zhang, P. Wu, Y. Li, L. Liao, Z. Fang, X. Zhong, ChemCatChem 2 (2010) 1115.

[29] T.K. Tseng, J. Choi, D.W. Jung, M. Davidson, P.H. Holloway, ACS Appl. Mater. Interfaces 2 (2010) 943.

[30] W. Li, Mater. Chem. Phys. 99 (2006) 174.

[31] M.G. Ma, J.F. Zhu, R.C. Sun, Y.J. Zhu, Mater. Lett. 64 (2010) 1524.

[32] T.P. Gujar, V.R. Shinde, D.D. Lokhande, R.S. Mane, S.H. Han, Appl. Surf. Sci. 252 (2006) 2747.

[33] T.P. Gujar, V.R. Shinde, C.D. Lokhande, Appl. Surf. Sci. 254 (2008) 4186.

[34] T. Takeyama, N. Takahashi, T. Nakamura, S. Itoh, Solid State Commun. 133 (2005) 771.

[35] H.W. Kim, J.W. Lee, S.H. Shim, Sens. Actuators B 126 (2007) 306.

[36] L. Li, Y.W. Yang, G.H. Li, L.D. Zhang, Small 2 (2006) 548.

[37] C. Wang, C. Shao, L. Wang, L. Zhang, X. Li, Y. Liu, J. Colloid Interface Sci. 333 (2009) 242.

Figure Captions

Figure 1. FESEM and TEM images of the precursor: (a) overall FESEM image, (b) magnified FESEM image, (c) typical TEM image, (d) magnified TEM image and (e) HRTEM image.

Figure 2. FESEM images of the precursor prepared at different hydrothermal temperature: (a) 180 °C, Bi^{3+}:CA molar ratio of 3:1, pH=6, 12 h and (b) 220 °C, Bi^{3+}:CA molar ratio of 3:1, pH=6, 12 h.

Figure 3. FESEM images of the precursor prepared with different reaction condition: (a) high concentration of CA (Bi^{3+}:CA molar ratio of 3:1, 200 °C, 12 h), (b) without CA (pH=6, 200 °C, 12 h), (c) hydrothermal process for 6 h (Bi^{3+}:CA molar ratio of 3:1, pH=6, 200 °C) and (d) hydrothermal process for 24 h (Bi^{3+}:CA molar ratio of 3:1, pH=6, 200 °C).

Figure 4. TGA and DTG curves of the precursor.

Figure 5. XRD patterns: (a) the precursor, (b) standard JCPDS data for $Bi_2(CO_3)O_2$, (c) as-prepared flower-shaped Bi_2O_3 and (d) standard JCPDS data for α-Bi_2O_3.

Figure 6. FESEM and TEM images of the Bi_2O_3 superstructure: (a) overall FESEM image, (b) magnified FESEM image, (c) typical TEM image, (d) magnified TEM image and (e) HRTEM image.

Figure 7. XPS spectra of the precursor and the flower-shaped Bi_2O_3: (a) survey scans and (b) Bi 4f narrow scans.

Figure 8. Morphological evolution of the flower-shaped precursor: hydrothermal process for (a) 2 h (with its TEM image in the inset), (b) 6 h and (c) 12 h.

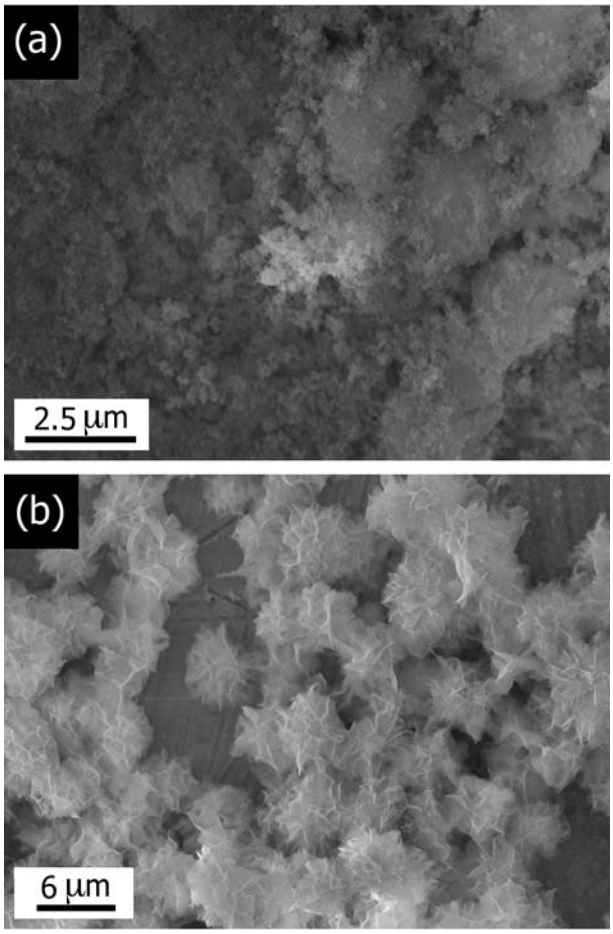

Figure 2.

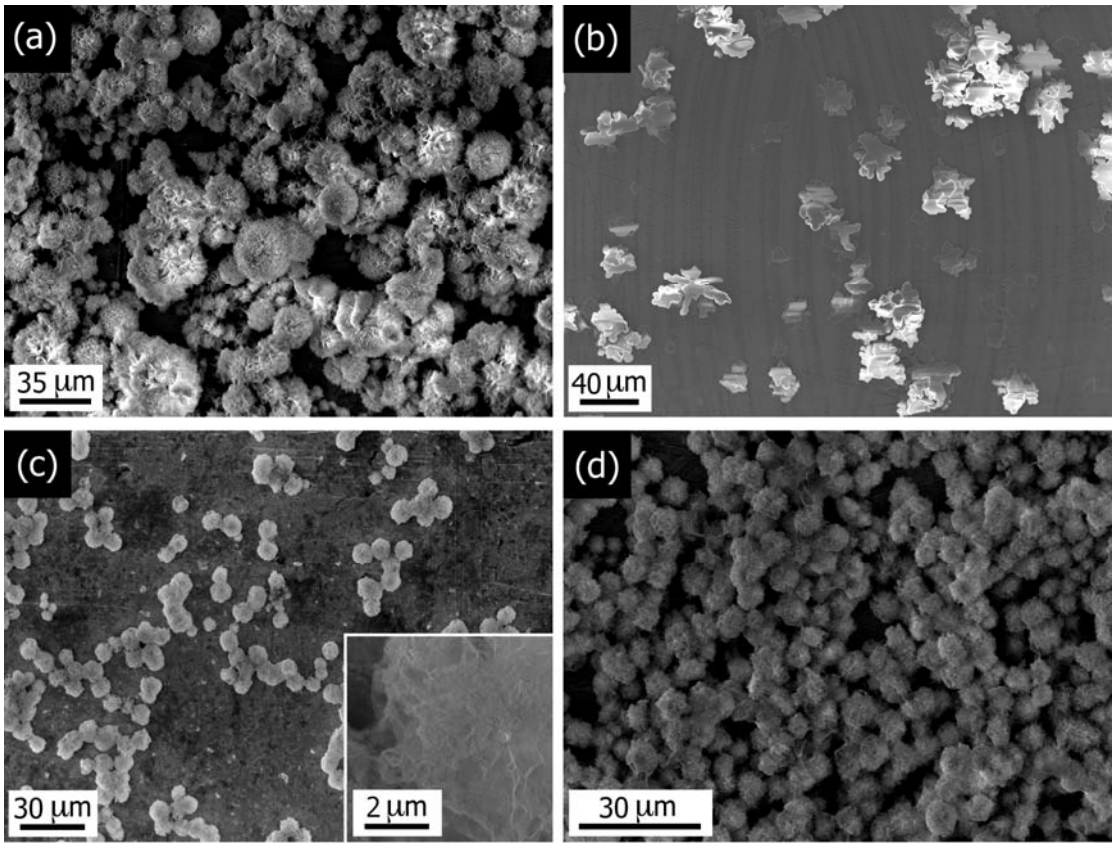

Figure 3.

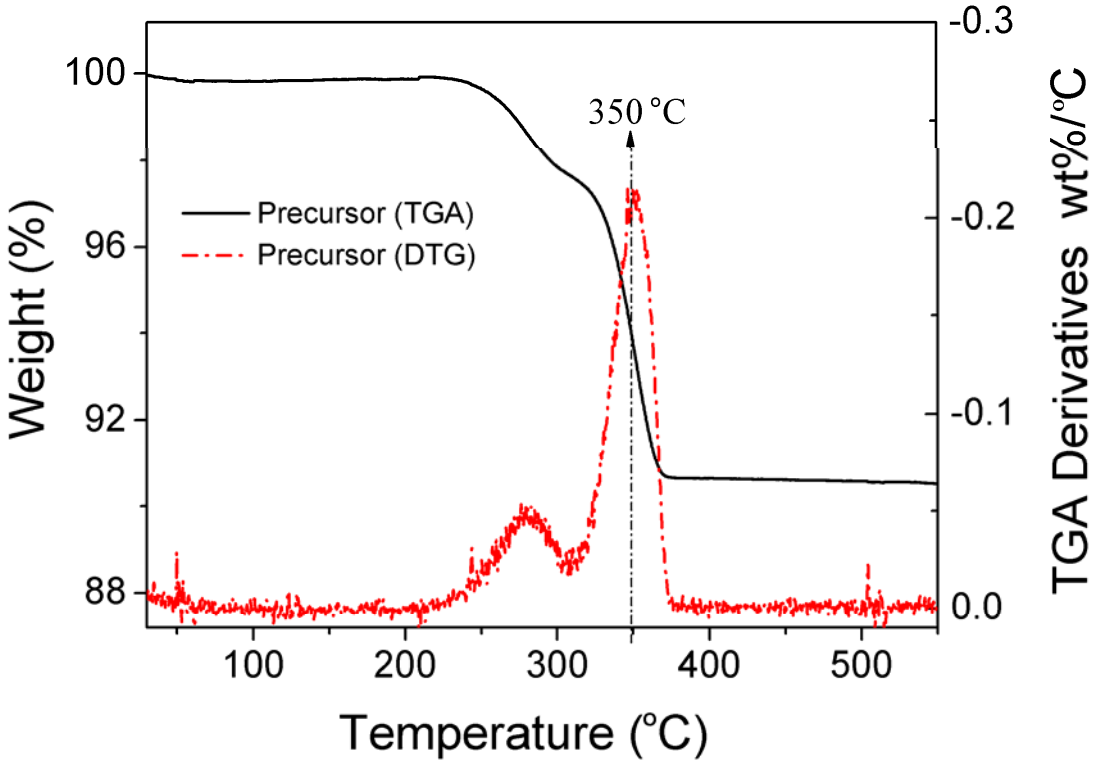
100
96
92
88
Weight (%)
350 °C
Precursor (TGA)
Precursor (DTG)
-0.3
-0.2
-0.1
0.0
TGA Derivatives wt%/°C
100
200
300
400
500
Temperature (°C)

Figure 4.

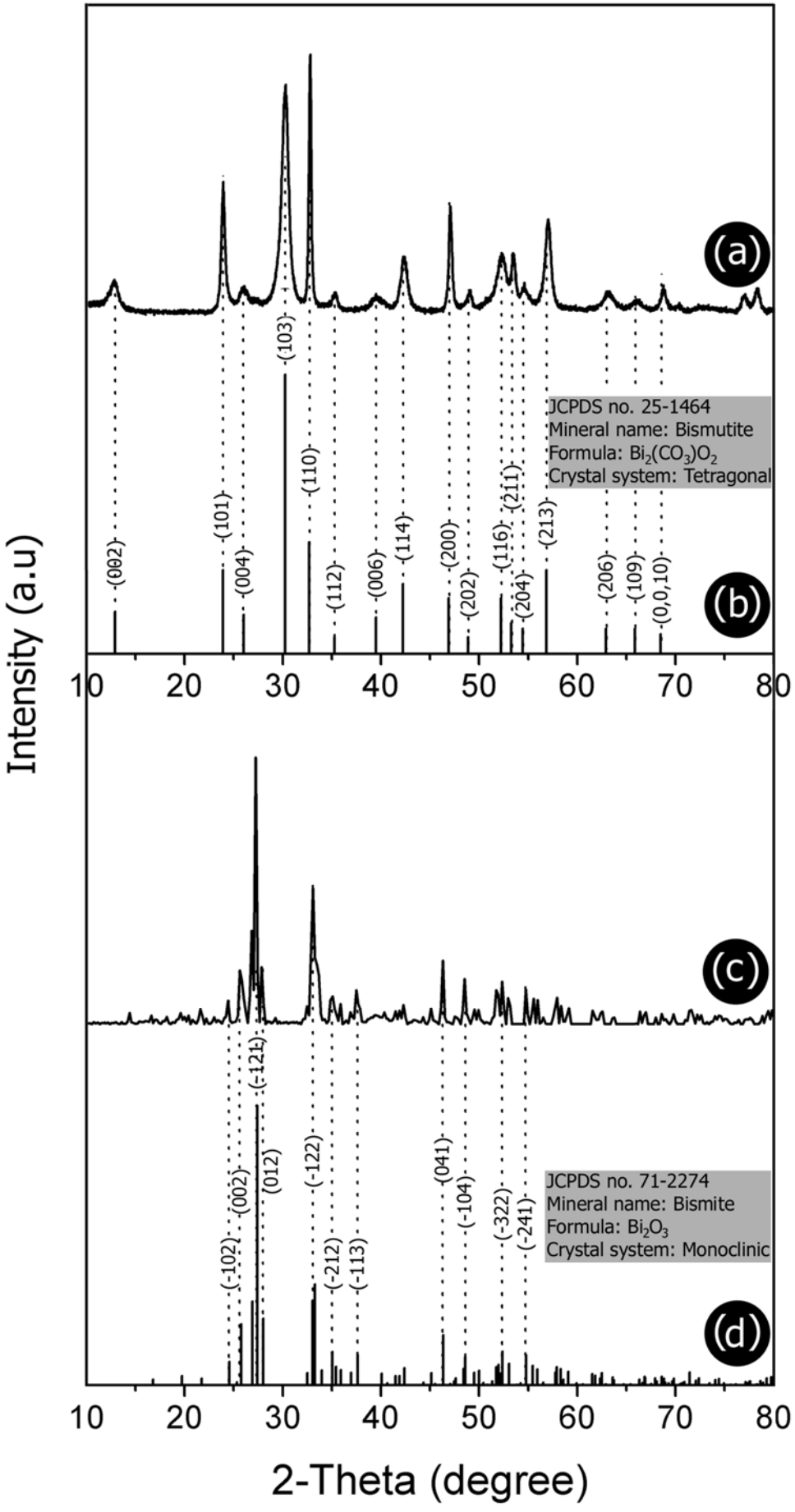
(a)
(b)
(c)
(d)
(002)
(101)
(004)
(103)
(110)
(112)
(006)
(114)
(200)
(202)
(116)
(211)
(204)
(213)
(206)
(109)
(0,0,10)
JCPDS no. 25-1464
Mineral name: Bismutite
Formula: $Bi_2(CO_3)O_2$
Crystal system: Tetragonal
(-102)
(002)
(-121)
(012)
(-122)
(-212)
(-113)
(041)
(-104)
(-322)
(-241)
JCPDS no. 71-2274
Mineral name: Bismite
Formula: Bi_2O_3
Crystal system: Monoclinic
Intensity (a.u)
10
20
30
40
50
60
70
80
2-Theta (degree)

Figure 5.

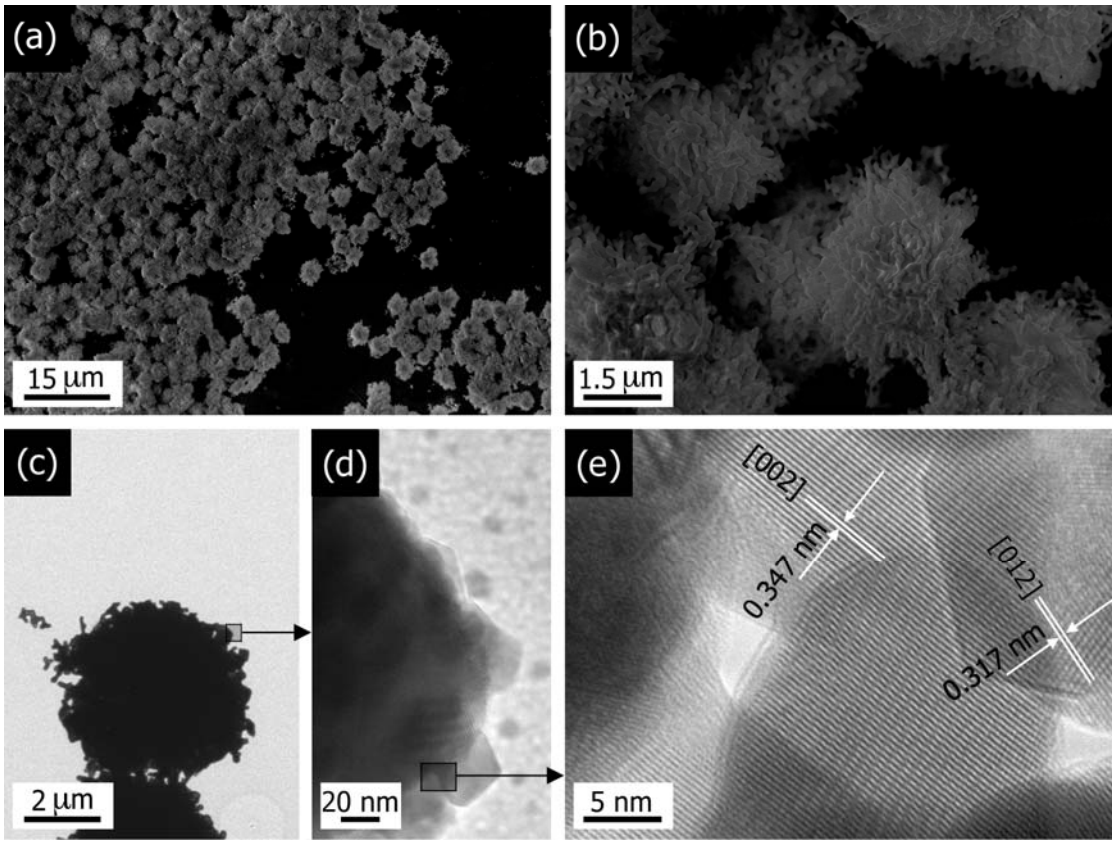

Figure 6.

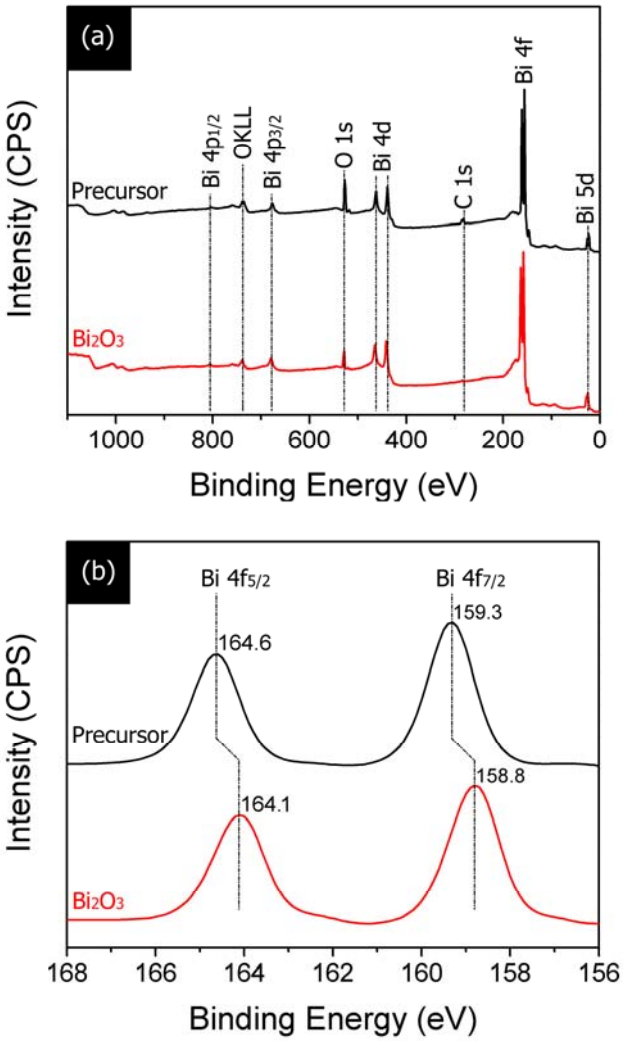
(a)
Intensity (CPS)
Precursor
Bi2O3
Bi 4p1/2
OKLL
Bi 4p3/2
O 1s
Bi 4d
C 1s
Bi 4f
Bi 5d
1000
800
600
400
200
0
Binding Energy (eV)
(b)
Intensity (CPS)
Bi 4f5/2
Bi 4f7/2
164.6
159.3
Precursor
164.1
158.8
Bi2O3
168
166
164
162
160
158
156
Binding Energy (eV)

Figure 7.

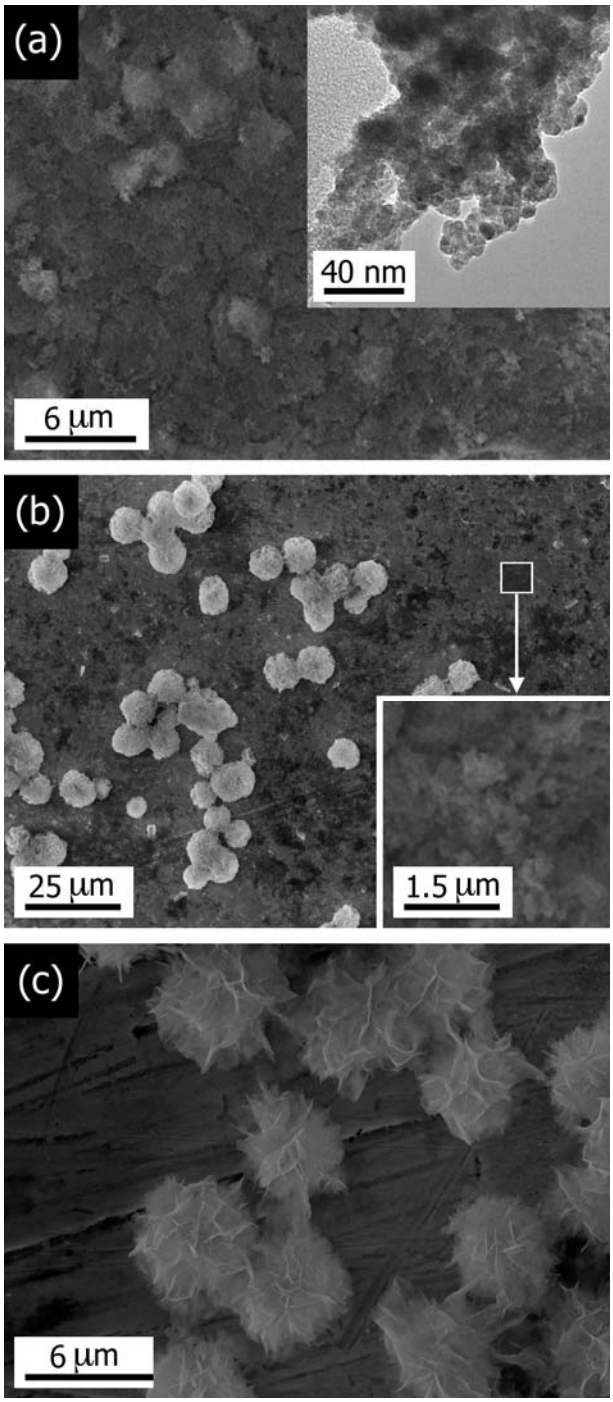

Figure 8.